High-repetition-rate pulsed electron source based on an atomic Rydberg photocathode

C. W. Rella and D. I. Duncan

Foundation for Fundamental Research on Matter (FOM), Institute for Atomic and Molecular Physics, Kruislaan 407, 1098 SJ Amsterdam, The Netherlands

F. Robicheaux

Department of Physics, 206 Allison Laboratory, Auburn University, Alabama 36849-5311

L. D. Noordam

Foundation for Fundamental Research on Matter (FOM), Institute for Atomic and Molecular Physics, Kruislaan 407, 1098 SJ Amsterdam, The Netherlands

Received May 1, 1998; revised manuscript received August 14, 1998

A gas of rubidium atoms has been excited by a combination of ultraviolet and far-infrared excitation to a superposition of Stark states lying just above the classical saddle point. Using an atomic streak camera, we have demonstrated that the atom ejects an ultrafast train of electron subpulses nearly equally spaced in time, with a repetition rate of approximately 50 GHz. The frequency characteristics of this pulse train are seen to be extremely sensitive to small changes in the static electric field. These measurements imply that, by variation of the electric field during the electron emission, it is possible to create shaped ultrafast electron pulses analogous to shaped optical pulses. © 1999 Optical Society of America [S0740-3224(99)00101-0]

OCIS codes: 020.0020, 020.5780, 320.5390, 320.7080, 320.7100, 320.0320.

The development of the atomic streak camera[1] has given researchers the ability to measure electron emission on a picosecond time scale. As a result, a great deal of theoretical and experimental effort has been devoted to the study of the time dependence of electron emission of highly excited alkali atoms in a strong electric field.[2–5] The creation of these Rydberg wave packets[6] can be accomplished in a variety of ways, the most common of which is laser excitation. The subsequent ionization of Rydberg states occurs because the electron has sufficient energy to overcome the classical potential energy barrier. However, because the excess energy is small, the electron is trapped in the vicinity of the atom for relatively long periods of time, up to hundreds of picoseconds. Temporal modulations of the electron flux arise from quantum-mechanical interference of the different energy components of the electron wave, corresponding to oscillations of the angular momentum of the electron.

Recently, it was predicted[7] that in principle an alkali atom in an electric field can be excited in such a way as to produce a long train of electron pulses (>10) with nearly uniform width and time separation. This is in contrast to short-pulse electron guns based on either photoactivated metal cathodes[8–11] or scattering of an electron beam by a short optical pulse,[12] which generally produce single electron pulses. The theory showed that the subpulse repetition frequency and overall envelope depends very sensitively on both the density of states in the region of excitation and the overlap between intermediate and final states.

There are therefore several ways by which the characteristics of electron emission can be modified. One can realize control of the emission by varying the laser excitation scheme, either by varying the energy or the bandwidth of the final step in the excitation process or by choosing different intermediate states. It has been found[13] that the dynamics of a Rydberg wave packet with a fixed energy and bandwidth can drastically be modified by creation of the wave packet by photoexcitation from different initial states. Changing the static electric field provides another method of varying the emission, by modification of the energy levels in a predictable fashion. Perhaps the most interesting feature of a Rydberg-atom-based electron gun is the possibility of controlling the electron period within the pulse train by varying the electric field during the emission process. It was shown[7] that the subpulse repetition rate can be altered by a factor of 3 while the electrons are being ejected. This implies that through appropriate control of experimental conditions it is possible to perform pulse shaping on electron pulses, which is analogous to the pulse shaping now performed on optical pulses.[14] Such pulses could be used, for example, to excite acoustic phonon modes on a surface, since the coupling to these modes would be large when the electron repetition frequency matches the phonon frequency. This type of electron spectroscopy could provide interesting complementary information to data obtained by other means, such as electromagnetic or acoustic spectroscopy, since phonons couple differently to electrons than to photons or other phonons.

0740-3224/99/010182-05$15.00

In this paper we present an experimental demonstration of a high-repetition-rate, Rydberg-atom-based electron gun.[15] Using an atomic streak camera with picosecond time resolution, we have measured the electron emission of highly excited rubidium atoms in a strong (1.7 kV/cm) electric field. Approximately ten evenly spaced subpulses of electrons are emitted, with an interpulse separation time of roughly 20 ps. In addition, it is shown that the repetition frequency (or carrier frequency) and the overall pulse envelope are strongly dependent on the electric-field strength. Changes as small as 0.6% ($\approx$10 V/cm) can produce dramatic changes in the character of the electron emission.

To fully characterize the operation of the Rydberg atom photocathode we have used an atomic streak camera,[1] the basic principles of which are presented here. Figure 1 depicts schematically the experimental apparatus, showing both the atomic streak camera itself and the optical excitation scheme. Rubidium atoms are evaporated from an oven in a vacuum system ($P \sim 10^{-7}$ Torr). These atoms drift into the interaction region between two metal plates, across which a voltage is placed. The electric field in the interaction region is approximately 1.7 kV/cm. Two lasers are used to prepare the appropriate Rydberg state. First, the atom is excited to the 16p state from the ground state by a frequency-doubled visible dye laser operating at 604.73 nm. This dye laser has a bandwidth of no greater than 1 cm^{-1} and a pulse a few nanoseconds long. The final laser in the excitation scheme is a far-infrared free-electron laser (FEL),[16] which excites the atoms to a superposition of states lying just above the classical saddle-point energy. The full capabilities of this FEL facility are described in detail elsewhere.[17] The FEL has a wavelength range of 5–100 μm and generates a pulse train of roughly 5000 pulses (called micropulses) of picosecond duration, separated by 1 ns. This pulse train (called a macropulse) is repeated at a 5-Hz repetition rate. For these experiments we used a single micropulse with an energy of approximately 1 μJ, and the laser was tuned to 27.1 μm with a fractional bandwidth ($\Delta\lambda/\lambda$) of roughly 0.5%, corresponding to a pulse length of approximately 10 ps.

The two laser beams counterpropagate through the interaction region perpendicular to the atomic beam. The far-infrared beam is transported from source to experiment entirely in vacuum to avoid the temporal distortions caused by propagation in air. Both lasers are polarized parallel to the static electric field. The frequency-doubled output of the dye laser is gently focused with a 50-cm lens to a spot somewhat smaller than 1 mm, and the FEL is focused to a spot a few millimeters in diameter. A narrow slit (300 μm wide $\times$ 1 cm long) is milled in one of the two electric-field plates. The emitted electrons are accelerated by the field and pass through this slit. The electrons then pass through two additional electric-field plates. The voltages on these plates are such that the finite interaction volume is brought to a time focus in the zero-field drift space beyond the final plate. In this drift space are a pair of deflection plates. A fast sweeping voltage is placed on these two plates by the rapid discharge of a large capacitor through a photoconductive GaAs switch. The switch is triggered by a seeded 5-Hz Nd:YAG laser synchronized within 50 ps of the FEL micropulses. The lifetime of the 16p state is long (hundreds of nanoseconds); therefore several FEL pulses contribute to the total photoionization signal, until the excited-state population is fully depleted. The voltages on these plates are arranged such that the photoionized electrons from only the first of these micropulses can proceed to the imaging system. The rapid electric-field ramp converts the longitudinal profile of the electron pulse (i.e., the time axis) into a transverse profile. The resulting electron image is amplified by a multichannel-plate charged-particle detector and is then imaged by a phosphor screen and a CCD camera. The data collected by the camera is digitized and recorded by a computer-controlled data-acquisition system. Multiple data sets were collected at the same experimental settings to verify the reproducibility of the results.

The intensity plot in Fig. 2 shows a typical single-shot streak camera image of the photoionization caused by a FEL micropulse. The horizontal axis is a true spatial axis along the direction of laser pulse propagation, whereas the vertical axis represents time, with the earliest times being given at the bottom of the image. Brightly colored regions indicate areas of higher electron flux. The optical pulse enters at the bottom left of this image and moves horizontally to the right. The strong diagonal band at the bottom of the image is caused by the initial ionized flux that is due to the incoming FEL pulse. The slope of this line is caused by the finite delay as the FEL pulse propagates across the field of view. From the

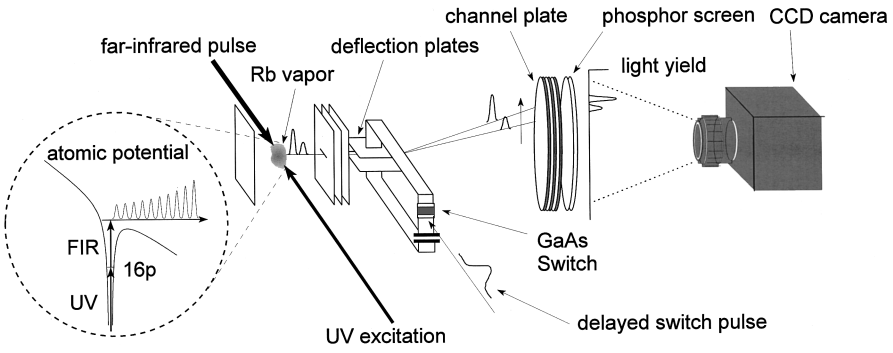

Fig. 1. Schematic showing the geometry of the interaction region and the basic operation of the atomic streak camera, together with a simple depiction of the optical excitation scheme.

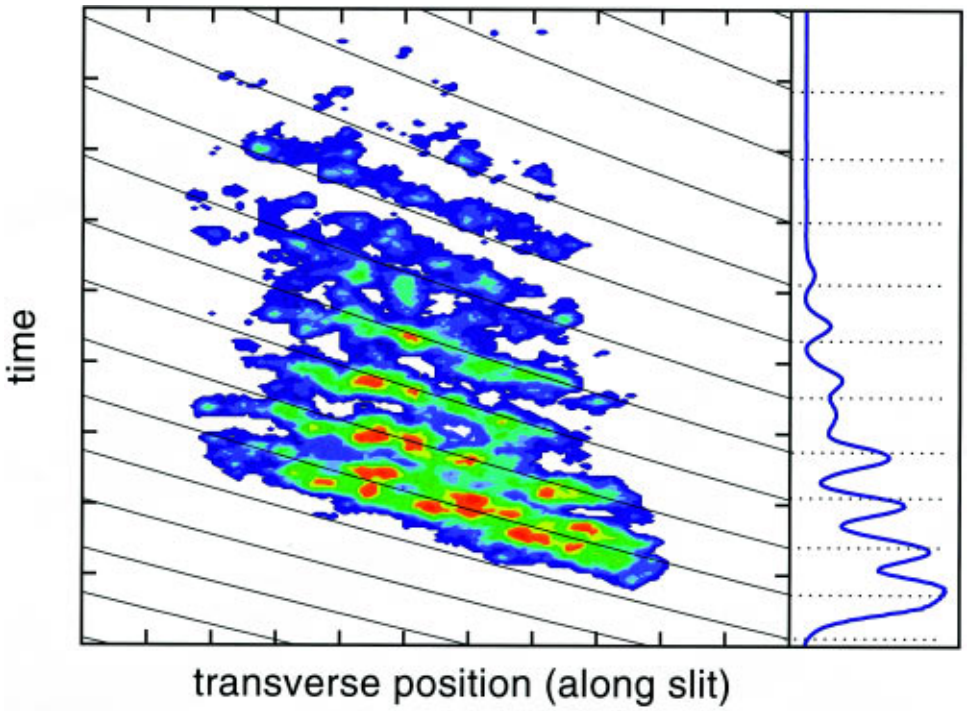

Fig. 2. Raw image, from the atomic streak camera, showing the modulated electron ionization due to a single ultrafast far-infrared pulse. The horizontal axis is distance parallel to the propagation of the laser beams, whereas the vertical axis represents the time axis due to the action of the time-varying electric field placed on the deflection plates. The image spans roughly 150 ps. This image was taken at a field strength of 1700 V/cm. The solid curves in the figure represent contours of constant time, with a separation of 30 ps between contours. At the right-hand side is a graph of the electron flux obtained by integration along contours of constant time.

slope of this line, the speed of light, and the known width of the slit, one obtains a calibration of the time axis.

Above this initial band are several additional bands of ionization, which are caused by the modulation of the ionization probability owing to interference between states of different energy in the excited wave function. The entire image has a duration of approximately 150 ps, whereas the duration of the excitation pulse of the FEL pulse is less than 10 ps. Clearly, the electron emission continues long after the optical pulse has arrived. No additional information is provided by the horizontal axis. It is therefore possible to integrate the signal along the diagonal bands to obtain a plot of the ionized electron flux as a function of time. This analysis is complicated by the fact that the slope of these bands increases somewhat at later times, which is due to the fact that the voltage ramp on the deflection plates is not perfectly linear in time. To this linear term we have therefore added a quadratic term to model the time-varying voltage ramp. The curves in Fig. 2 represent lines of constant time. The parameters of the voltage ramp are chosen empirically such that the recurrences of the electron flux run parallel to these lines. In this process there is some uncertainty, which leads to a slight ($<10\%$) uncertainty in the time axis, especially at later emission times. However, since we collected all the data without changing the parameters of the switching field, we analyzed the data by using the same parameters for the voltage ramp.

At the right-hand side of Fig. 2 the results of integration along the time contours can be seen. The modulations in the raw data are clearly evident in the time dependence of the electron flux. Note that the time axis is not linear, which is due to the nonlinearity of the voltage ramp. These same data are displayed with a properly reconstructed time axis in the central panel of Fig. 3. For this particular set of experimental parameters there are at least eight electron subpulses, spaced approximately evenly in time. The subpulse spacing is 20 ps; hence the electron gun has a 50-GHz repetition frequency.

Previous theoretical and experimental work[18] has demonstrated that the ionization probability is strongly dependent on the angular momentum of the wave packet. In a static electric field the angular momentum can be shown to oscillate between low and high values with a period τ given by

$$\tau = \frac{2\pi}{3Fn}, \tag{1}$$

where n is the principle quantum number and F is the electric-field strength in atomic units. The probability for ionization is significantly enhanced at low l because the scattering probability off the core is enhanced and because the radial velocity is maximal. Therefore the ionization probability is also modulated with a period τ. However, the radial oscillation time, or orbit period, given by $2\pi n^3$, is also important, since for core scattering to occur the electron must be in the vicinity of the core when the angular momentum is low.[3,19] Thus enhancement in the electron yield occurs at recurrence times between these two frequencies. For these experiments the angular oscillation time is 7.8 ps, assuming that blue-shifted

Stark states are excited. To scatter from the Rb^+ core the angular and radial recurrence must be quite precise. Apparently, since the electron subpulse repetition frequency is roughly 20 ps, this condition is satisfied every third angular-momentum oscillation. It is important to remember that the above arguments are strictly valid only for a hydrogenic atom at electric-field levels below the point at which the different n manifolds of Stark states begin to mix. Nevertheless, this simple treatment provides useful insight into the physical mechanisms governing the electron emission.

Small changes in the electric field placed on the atoms can dramatically change the dynamics of electron emission. In Fig. 3, two streak traces taken at 1690 and 1705 V/cm, respectively, are displayed along with the streak trace taken at 1700 V/cm. Vertical dashed lines indicate the peak positions of the central 1700-V/cm trace. Note that not only the overall envelope but also the repetition frequency of the subpulses change between different traces (the former changes dramatically). Especially interesting is the top trace, taken at 1690 V/cm, where a second, slower oscillation frequency is also evident in the electron emission.

In general, atoms excited to the vicinity of the saddle point do not exhibit the pulsed emission shown in Fig. 3. Only for specific schemes of excitation does the atom behave in this manner. Thus, to develop a practical source for shaped electron bunches, it is necessary to be able to predict with the theory where the most fruitful regions of parameter space will lie. The calculated electron flux

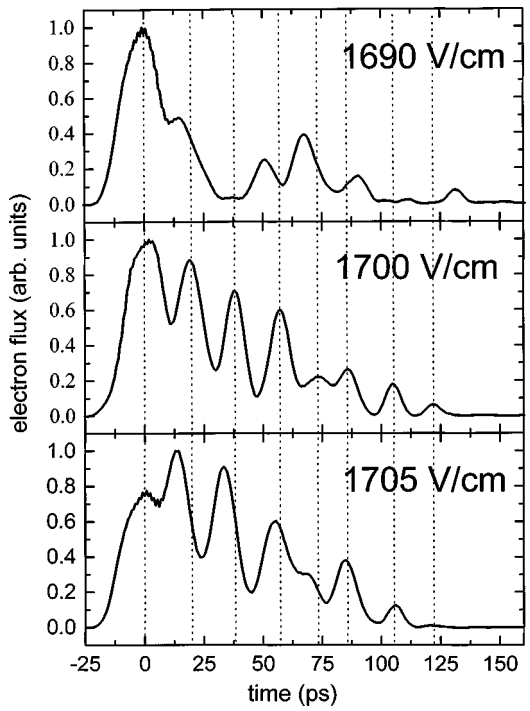

Fig. 3. Reconstructed ionization traces obtained at three different field strengths, respectively (from the top): 1690, 1700, and 1705 V/cm. All the other experimental parameters remained unchanged. The vertical dotted lines are provided to guide the eye. The observed variations in carrier frequency and envelope are due primarily to changes in the overlap between the excitation spectrum and the Stark state energies caused by the changing electric field.

was obtained by the method described in previously published work.[4,5,13] It is assumed that the FEL only perturbatively excites the atom from its initial Rydberg state, so first-order time-dependent perturbation theory may be used. The excited part of the wave function is obtained numerically with

$$i\partial\psi/\partial t - H\psi = G(t)\exp(-i\omega t)D\ \exp(-iE_0 t)\psi_0, \quad (2)$$

where H is the atom-plus-static-electric-field Hamiltonian, ω is the central laser frequency, $G(t)$ is the laser envelope, D is the dipole operator, E_0 is the initial state energy, and Ψ_0 is the initial state. This equation is solved by expansion of ψ in a basis of radial functions and spherical harmonics that are eigenstates of the atomic Hamiltonian that go to zero at a distance of 2700 a.u. Reflection from this boundary is prevented by use of a mask. The time-dependent coefficients of the basis functions are obtained with the staggered leapfrog algorithm.[20] We calculate the flux at each time, using

$$\mathcal{F}(t) = \mathrm{Im}\left[\int \mathrm{d}\Omega\,\psi^*(\mathbf{r}, t)\,\frac{\partial\psi}{\partial r}(\mathbf{r}, t)\right], \quad (3)$$

with $\mathbf{r}$ being chosen to be larger than the distance to the saddle point. This methodology allowed us to efficiently use massively parallel computers to obtain the wave function.

In the experiment the initial state was an admixture of $m = 1$ and $m = 0$ character (m is the azimuthal quantum number) because of the spin-orbit interaction. However, the spin-orbit interaction does not affect the final state over the time scales investigated in the experiment. The total flux was calculated by performance of two runs on each set of experimental parameters: One run was with $m = 0$ final states, and one run was with $m = 1$ final states. The total flux is the incoherent sum of the fluxes from the two m final states, with the appropriate weights, reflecting the m character of the initial state. For the calculated results at 1700 V/cm the $m = 0$ to $m = 1$ ratio is 1:2.

In Fig. 4 we compare the same data shown in the central panel of Fig. 3 together with the results of theoretical modeling. Similar agreement can be obtained throughout the range of electric fields measured in the experiment. It is important to note that, although there are discrepancies, the theory not only reproduces the pulsed behavior of the emission but also correctly predicts the frequency of the modulation. It is thus possible to identify interesting regions by use of the theory without having to resort to experimental exploration of the full parameter space.

However, the agreement between experiment and calculation is not perfect. It is clearly very good in the initial stages of pulse evolution, although with increasing time delay the agreement becomes less satisfactory. One problem is that the theory appears to overestimate the size of the ionization at long times (>100 ps). This is because the electron imaging system after the deflection plates has a finite acceptance size, which limits the total time duration that can be recorded. Furthermore, the later flux peaks seem to occur at somewhat different

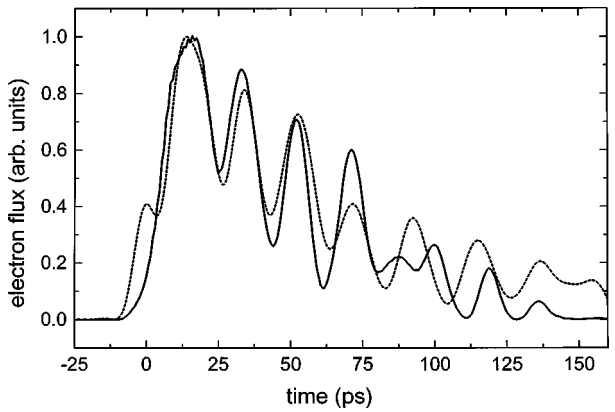

Fig. 4. Comparison between data collected at 1700 V/cm (shown in the central panel of Fig. 3) and theoretical modeling. The static electric field, the far-infrared laser center frequency, the bandwidth, and the chirp were varied within experimental uncertainty to yield reasonable agreement between model and data. Deviations between data and theory at long times is due to the extreme sensitivity of the experiment to small variations in the optical spectrum and the electric field (see text).

times than is predicted. These errors in pulse emission times are of the order of 10 ps at a time 80 ps after the initial excitation, and thus they correspond to errors in energy spacings of just 0.2 cm^{-1}.

The main difficulty in modeling the data arises from two sources, both of which limit the accuracy at long times: uncertainty in the experimental parameters used as input into Eq. (2), and uncertainty in the calculations. There are four experimental parameters that are used as input into Eq. (2): (a) the static-electric-field strength, (b) the main laser frequency ω, (c) the optical pulse profile $G(t)$, and (d) the chirp of the laser pulse. Measurement of these parameters with an accuracy sufficient to obtain a precise match between theory and experiment at long times is highly impractical. These input parameters for Eq. (2) were varied within the experimental uncertainties until a decent match between calculated and experimental flux was obtained. However, the time-consuming nature of the calculations prevented a thorough search of the parameter space. Furthermore, errors in the calculation that are due to uncertainty in the model potential used to calculate the dynamics of the Rydberg electron may be contributing to the discrepancy at long times through small errors in energy positions and oscillator strength. Finally, neglecting the spin-orbit interaction in the calculation may also contribute to deviations at long times. This is unlikely, however, since the dominant contribution to the spin-orbit coupling is the p state, which, after being distributed across the n manifold, induces a spin-orbit precession that is much longer than the time scale investigated here.

In conclusion, we have demonstrated experimentally the formation of electron pulses with complex substructure by the photoionization of rubidium atoms by a single far-infrared pulse. It is further shown that the carrier frequency of these subpulses can be dramatically modified in a predictable fashion through minute ($<1\%$) variations in the electric field applied to the rubidium atoms. These measurements imply that, through the careful application of time-varying electric fields, shaped electron pulses of variable carrier frequency and overall envelope can be generated and characterized. These shaped pulses, analogous to the shaped optical pulses now generated from ultrafast lasers, can then be used for the study of a variety of resonant processes in the gigahertz frequency regime.

ACKNOWLEDGMENTS

We gratefully acknowledge the assistance of A. F. G. van der Meer, G. M. H. Knippels, and the rest of the support team at the Free Electron Laser for Infrared eXperiments facility, Foundation for Fundamental Research on Matter- (FOM-) Rijnhuizen. F. Robicheaux's work is supported by the National Science Foundation. Computational work was carried out at the National Energy Research Supercomputer Center in Berkeley, California. This work is part of the research program of the Stichting voor Fundamenteel Onderzoek der Materie (Foundation for Fundamental Research on Matter) and was made possible by financial support from the Nederlandse Organisatie voor Wetenschappelijk Onderzoek (Netherlands Organization for the Advancement of Research) and the Technology Foundation.

REFERENCES AND NOTES

1. G. M. Lankhuijzen and L. D. Noordam, Phys. Rev. Lett. **76**, 1784 (1996).
2. G. M. Lankhuijzen and L. D. Noordam, Phys. Rev. A **52**, 2016 (1995).
3. C. Raman, T. C. Weinacht, and P. H. Bucksbaum, Phys. Rev. A **55**, R3995 (1997).
4. F. Robicheaux and J. Shaw, Phys. Rev. Lett. **77**, 4154 (1996).
5. F. Robicheaux and J. Shaw, Phys. Rev. A **56**, 278 (1997).
6. For a review of the physics of Rydberg atoms, see, for example, Thomas F. Gallagher, *Rydberg Atoms* (Cambridge U. Press, Cambridge, UK, 1994).
7. F. Robicheaux, G. M. Lankhuijzen, and L. D. Noordam, J. Opt. Soc. Am. B **15**, 1 (1998).
8. H. E. Elsayed-Ali and J. W. Hermann, Rev. Sci. Instrum. **61**, 1636 (1990).
9. J. C. Williamson, M. Dantus, S. B. Kim, and A. H. Zewail, Chem. Phys. Lett. **196**, 529 (1992).
10. G. Farkas and C. Toth, Phys. Rev. A **41**, 4123 (1990).
11. D. M. Riffe, X. Y. Wang, Michael C. Downer, D. L. Fisher, T. Tajima, J. L. Erskine, and R. M. More, "Femtosecond thermionic emission from metals in the space-charge-limited regime," J. Opt. Soc. Am. B **10**, 1424 (1993).
12. V. G. Minogin, M. V. Fedorov, and V. S. Letokhov, Opt. Commun. **140**, 250 (1997).
13. G. M. Lankhuijzen, M. Drabbels, F. Robicheaux, and L. D. Noordam, Phys. Rev. A **57**, 440 (1998).
14. A. M. Weiner, J. P. Heritage, and E. M. Kirschner, J. Opt. Soc. Am. B **5**, 1563 (1988).
15. For a description of a Rydberg atom-based low-energy electron gun, see D. Klar, M.-W. Ruf, and H. Hotop, Meas. Sci. Technol. **5**, 1248 (1994).
16. A detailed treatment of the theory of FEL operation can be found, for example, in C. A. Brau, *Free Electron Lasers* (Academic, Boston, Mass., 1990), 51ff.
17. D. Oepts, A. F. G. van der Meer, and P. W. van Amersfoort, Infrared Phys. Technol. **36**, 297 (1995).
18. L. D. Noordam, A. ten Wolder, and A. Lagendijk, "Time de-

pendence of an atomic electron wave function in an electrical field," Phys. Rev. A **40**, 6999 (1989).
19. G. M. Lankhuijzen, F. Robicheaux, and L. D. Noordam, Phys. Rev. Lett. **79**, 2427 (1997).
20. W. H. Press, S. A. Teukolsky, W. T. Vetterling, and B. P. Flannery, *Numerical Recipes* (Cambridge U. Press, Cambridge, UK, 1992).